Diameter Dependence of Scattering Limited Transport Properties of Si Nanowire MOSFETs under Uniaxial Tensile Strain

Takahisa Tanaka and Kohei M. Itoh
School of Fundamental Science and Technology, Keio University
3-14-1 Hiyoshi, Kohoku-ku, Yokohama 223-8522, Japan

***Abstract*—Effects of the diameter on the drain current of uniaxially strained Si nanowire (NW) MOSFETs are investigated. Based on the deterministic solution of the multi-subband Boltzmann transport equation, the drain current is calculated considering the intravalley acoustic phonon scatterings, intervalley phonon scatterings and interface roughness scatterings. We found 3 nm diameter [110] oriented Si NW MOSFETs shows ~2× drain current enhancement by the 1% uniaxial tensile strain.**

Keywords—nanowire; silicon; uniaxial strain; MOSFET;

I. Introduction

Integration of Si MOSFETs has been realized by down scaling. However, with the down scaling reaching the several 10 nm region, the short channel effects are becoming problems. To avoid this short channel effects, Si nanowire (NW) MOSFETs have attracted much attention. The experimentally reported mobility of Si NW MOSFETs, however, is lower than the universal mobility obtained for the bulk MOSFETs [1]-[3]. This indicates that the mobility in the currently available Si NW MOSFETs is limited by the strong carrier scattering even for the gate length as short as 10 nm [4], [5]. In order to overcome this shortcoming, introduction of strains in the channel is expected to be effective for the reduction of the transport effective mass and the suppression of carrier scattering in Si NW MOSFETs. In previous work, the size dependence of the drain current enhancement by the uniaxial tensile stress has been investigated for the ballistic transport regime [6]. The present work investigate theoretically scattering limited transport properties of cylindrical Si NW MOSFETs under the fixed uniaxial tensile strain in [100] and [110] directions, and the effect of the diameters between 3 and 8 nm were studied.

II. Calculation Method

A. Device and Band Structure

Fig. 1 (a) shows a schematic diagram of simulated [100] and [110] oriented cylindrical Si NW MOSFETs. The drain voltage is fixed at 0.65 V. The 10 nm long channel region is undoped and surrounded by the 0.5 nm thick Si dioxide and gate. 10 nm long source and drain regions are heavily doped N_D=10^{20} cm^{-3} n-type Si. The difference of the work function between gate and source is neglected. Fig. 1 (b) and Fig. 1 (c) show conduction valleys in the confinement plane perpendicular to the transport direction. To represent the band structure, we employ the effective mass approximation with parabolic bands. For the [100] transport, effective masses are ($m_{v;x}$, $m_{v;y}$,$m_{v;z}$)=(0.19, 0.19, 0.916) for v=1, 2, ($m_{v;x}$, $m_{v;y}$, $m_{v;z}$)=(0.19, 0.916, 0.19) for v=3, 4 and ($m_{v;x}$, $m_{v;y}$,$m_{v;z}$)=(0.916, 0.19, 0.19) for v=5, 6. On the other hand, for the [110] transport, ($m_{v;x}$, $m_{v;y}$,$m_{v;z}$)=(0.23, 0.916, 0.19) for v=1, 2, ($m_{v;x}$, $m_{v;y}$,$m_{v;z}$)=(0.315, 0.19, 0.553) for v=3-6. The effective mass along the x-axis for valleys with v=1, 2 is modified because of the strong nonparabolicity [7].

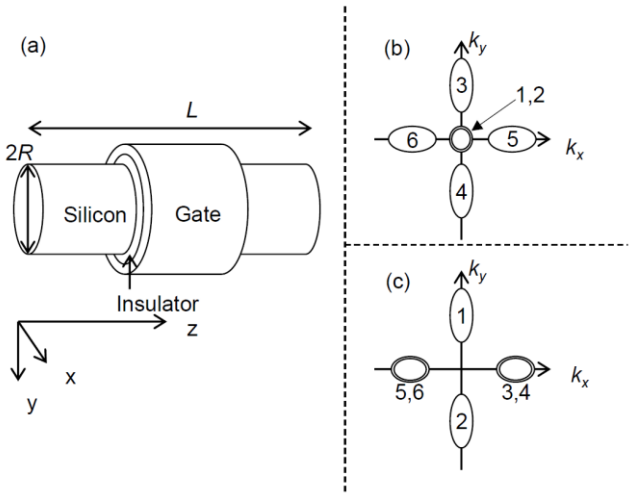

Fig. 1. (a) Schematic diagram of a Si nanowire MOSFET with coordinate axes. Projection of conduction valleys to the perpendicular plane to the (b) [100] and (c) [110]. The valley index v=1-6 is also shown.

B. Current-Voltage Characteristics

Drain current-gate voltage (I_D-V_G) characteristics are calculated based on the self-consistent solver of the Poisson, Schrödinger and multi-subband Boltzmann transport equation [4], [5]. In order to treat the energy levels of subbands, the anisotropic effective mass tensor rather than isotopically approximated effective mass is employed for solving the two-dimensional Schrödinger equation. The uniaxial tensile strain of 1% along the transport direction is assumed in the same way as the bulk silicon [8] with the deformation potential given in [9]. In calculations of the multi-subband Boltzmann

This work was supported by Grant-in-Aid for JSPS Fellows and JST-CREST.

transport equation, electron scatterings by intravelley acoustic phonons, intervalley phonons and interface roughness are taken into account. Deformation potentials of phonon scatterings are taken from Table II of [5]. The scattering matrix element from the nth subband to the n'th subband by interface roughness scattering is calculated by the Fourier series expansion [10]:

$$\left\langle \left| V^{SR}_{q_z;n,n'} \right|^2 \right\rangle = \sum_l \left| \Gamma_{l;n,n'} \right|^2 \frac{C(l,q_z)}{RL}, \quad (1)$$

$$\Gamma_{l;n,n'} = R\int \frac{\hbar^2 m_\phi}{2} \left(\mathbf{n}\cdot\mathbf{M}^{-1}\cdot\nabla\psi^*_{n'}\right)\left(\mathbf{n}\cdot\mathbf{M}^{-1}\cdot\nabla\psi_{n'}\right) \times \exp(il\phi)d\phi, \quad (2)$$

where m_ϕ is the polar angular dependent effective mass determined by $m_{v;\phi}=1/[\cos^2\phi/m_{v;x}+\sin^2\phi/m_{v;y}]$, $\mathbf{n}$ is the unit vector perpendicular to the NW surface at the polar angular ϕ, $\mathbf{M}$ is the anisotropic effective mass tensor, ψ_n [$\psi_{n'}$] is the wavefunction of the nth [n'th] subband, and $C(l,q_z)$ is the Gaussian type power spectrum of interface roughness defined by,

$$C(l,q_z) = \pi\Delta^2\Lambda^2 \exp\left[-\frac{\left(l^2/R^2+q_z^2\right)\Lambda^2}{4}\right], \quad (3)$$

where Δ=0.3 nm is the rms of roughness height and Λ=1.5 nm is the correlation length of interface roughness. In the insulator, we neglect the polar angular dependence of the wavefunction and assume the penetration of the wavefunction is negligibly small.

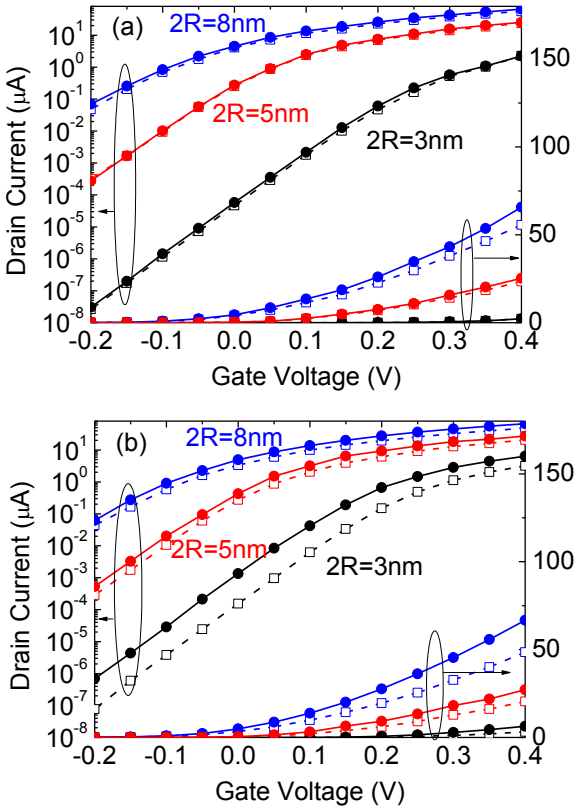

Fig. 2 Calculated I_D-V_G characteristics of strained (filled circles and solid lines) and unstrained (open squares and dashed lines) Si NW MOSFETs for transport directions (a) [100] and (b) [110]. Diameters of NWs $2R$= 3 nm (black), 5 nm (red) and 8 nm (blue).

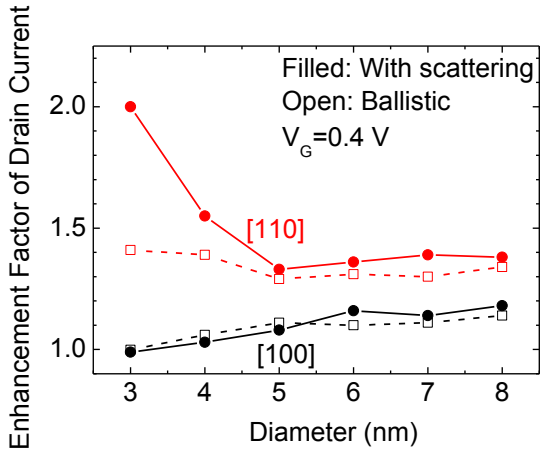

Fig. 3 Diameter dependence of the enhancement factor for [100] (black symbols) and [110] (red symbols) oriented Si NW MOSFETs at the gate voltage V_G=0.4 V.

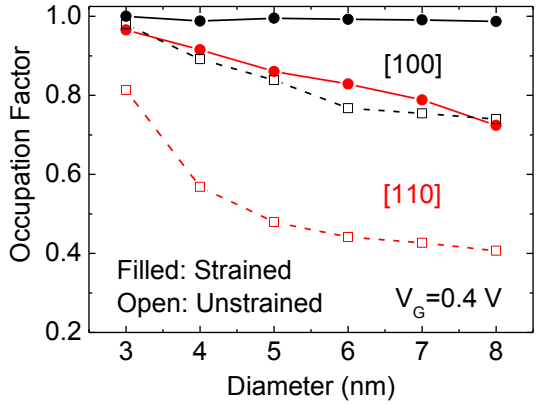

Fig. 4 Diameter dependence of occupation factor with the gate voltage V_G=0.4 V. Occupation factors for strained (filled circles and solid lines) and unstrained (open squares and dashed lines) Si NW MOSFETs with transport directions [100] (black) and [110] (red) are shown.

III. Result and Discussion

Figs. 2 (a) and (b) show calculated I_D-V_G characteristics of strained (1% uniaxial tensile strain) and unstrained Si NW MOSFETs with the NW diameter $2R$=3, 5 and 8 nm. From Figs. 2 (a) and (b), a large enhancement of the I_D can be seen for [110] oriented Si NW MOSFETs, while I_D-V_G characteristics for [100] oriented Si NW MOSFETs show a small enhancement by the uniaxial tensile strain. To investigate the diameter dependence, the enhancement factor of the drain current defined by $I_{D,\text{strained}}/I_{D,\text{unstraind}}$ at V_G=0.4 V is shown in Fig. 3. The enhancement factor calculated from ballistic transport for [100] and [110] oriented Si NWs are also shown. Here, we discuss two points: the different diameter dependence between [100] and [110] oriented Si NW MOSFETs, and the difference between the scattering limited and ballistic transport for [110] oriented Si NW MOSFETs.

The difference between [100] and [110] oriented Si NW MOSFETs is originating from and change of the transport

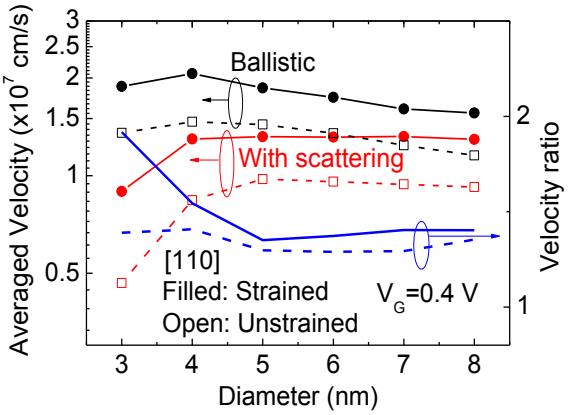

Fig. 5 Diameter dependence of averaged carrier velocity with the gate voltage V_G=0.4 V. Carrier velocities for strained (filled circles and solid lines) and unstrained (open squares and dashed lines) Si NW MOSFETs with scattering (red) and for ballistic (black) are shown. Ratios between averaged velocities with and without the uniaxial tensile strain for ballistic (blue dashed line) and scattering limited (blue solid line) transports are also shown.

effective mass and the valley occupation by the uniaxial tensile strain. According to [8], the uniaxial tensile strain reduces the transport effective mass of valleys v=1, 2 for [110] oriented Si NW MOSFETs, while there is no change of the transport effective mass for [100] oriented Si NW MOSFETs. This causes the lower enhancement factor for the [100] transport than that for the [110] transport. In addition to this, the small change in the carrier occupation for each valleys causes the small enhancement factor of the small diameter ($2R$ < 6 nm) [100] oriented Si NW MOSFETs. Fig. 4 shows the occupation factor of valleys with v=3-6 for [100] and v=1, 2 for [110] oriented Si NW MOSFETs. These valleys have a small transport effective mass 0.19. The occupation factor is determined from the number of electrons in these valleys divided by the number of total electrons inside the simulated Si NW MOSFETs. The increase of the occupation factor by strain means the reduction of transport effective mass and the enhancement of I_D. In case of [100] oriented Si NW MOSFETs, the change in the occupation factor by the uniaxial tensile strain is small compared to [110], because the large degeneracy of the lower valleys v=3-6 makes the occupation factor large even without strain.

The large enhancement of scattering limited I_D in [110] oriented Si NW MOSFETs by strain is mainly caused by the increase of carrier velocity. Fig. 5 shows the diameter dependence of the carrier velocity averaged along the transport direction. When scatterings present, the carrier velocity is lowered from the carrier velocity of the ballistic transport. On the other hand, the ratio between scattering limited carrier velocities with and without the uniaxial tensile strain is larger than the ratio of carrier velocities for ballistic transport, because the uniaxial tensile strain changes the scattering amplitude via the change of the valley occupation as shown in Fig. 4. The largest change of carrier velocity is observed for [110] oriented Si NW MOSFETs with the 3 nm diameter. This originates from the subband occupation. Figs. 6 (a) and (b) shows the diameter dependence of the subband occupation factor and the averaged carrier velocity of each subband. The subband occupation factor is defined as the ratio

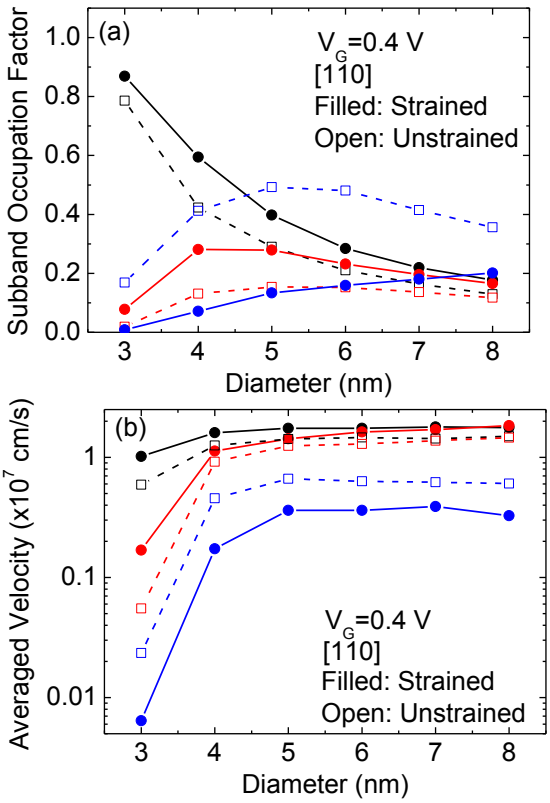

Fig. 6 Diameter dependence of (a) the subband occupation factor and (b) the averaged velocity for each subband with the gate voltage V_G=0.4 V. Symbols and lines represent the occupation factor for strained (filled circles and solid lines) and unstrained (open squares and dashed lines) Si NW MOSFETs, and the color represents the first (black) and second (red) subbands of valleys v=1, 2, and the first subband of valleys v=3-6 (blue).

between the number of electrons in the certain subband and the number of total electrons inside the simulated Si NW MOSFET. By applying the uniaxial tensile strain, electrons are transfered from valleys v=3-6 to valleys v=1, 2 as shown in Fig. 4 and Fig. 6 (a). When the diameters are between 4 nm and 8 nm, electrons move from valleys v=3-6 to first, second and higher subbands of valleys v=1, 2 by the uniaxial tensile strain. When the diameter is 3 nm, electrons move mainly to the first subband of valleys v=1, 2 due to the strong quantum confinement. Fig. 6 (b) shows that the second subband of valleys v=1, 2 has lower carrier velocities compared to that in the first subband. The suppression of the occupation of the second subband causes the large increase of the carrier velocity and enhancement factor.

IV. Conclusion

We have investigated the diameter dependence of scattering limited carrier transports in uniaxially strained Si NW MOSFETs. The enhancement of I_D for the quasi-ballistic transport in [110] oriented Si NW MOSFETs is larger than the enhancement for the ballistic transport; I_D can be increased twice by the uniaxial tensile strain for [110] oriented Si NW MOSFETs when diameter is set at 3 nm. This has been achieved by the change of the scattering amplitude with suppression of the occupation of the second subband.

REFERENCES

[1] S. Takagi, A. Toriumi, and H. Tango, "On the universality of inversion layer mobility in Si MOSFETs; Part I-Effects of substrate impurity concentration," IEEE Trans. Electron Devices, vol. 41, pp. 2357-2362, 1994.

[2] O. Gunawan, L. Sekaric, A. Majumdar, M Rooksm J. Aooenzeller, J. W. Sleight, S. Guha, and W. Haensch, "Measurement of carrier mobility in silicon nanowires," Nano Lett., vol. 8, pp. 1567-1571, 2008.

[3] J. Chen, T. Saraya, K. Miyaji, K. Shimizu, and T. Hiramoto, "Experimental study of mobility [110]- and [100]-directed multiple silicon nanowire GAA MOSFETs on (100) SOI," VLSI Tech., pp. 32-33, 2008.

[4] S. Jin, M. V. Fischetti, and T. –W. Tang, "Theoretical study of carrier transport in silicon nanowire transistors based on the multisubband Boltzmann transport equation," IEEE Trans. Electron Devices, vol. 55, pp. 2886-2897, 2008.

[5] M. Lenzi, P. Palestri, E. Gnani, S. Reggiani, A. Gnudi, D. Esseni, L. Selmi, and G. Baccarani, "Investigation of the transport properties of silicon nanowires using deterministic and Monte Carlo approaches to the solution of the Boltzmann transport equation," IEEE Trans. Electron Devices, vol. 55, pp. 2086-2096, 2008.

[6] L. Zhang, H. Lou, J. He, and M. Chan, "Uniaxial strain effects on electron ballistic transport in gate-all-around silicon nanowire MOSFETs," IEEE Trans. Electron Devices, vol. 58, pp. 3829-3836, 2011.

[7] N. Serra, and D. Esseni, "Basic insight about the strain engineering of n-type FinFETs," ULIS, pp. 113-116, 2009.

[8] E. Ungersboeck, S. Dhar, G. Karlowatz, V. Sverdlov, and H. Kosina, "The effect of general strain on the band structure and electron mobility of silicon," IEEE Trans. Electron Devices, vol. 54, pp. 2183-2190, 2007.

[9] M. V. Fischetti, and S. E. Laux, "Band structure, deformation potentials, and carrier mobility in strained Si, Ge, and SiGe alloys," J. Appl. Phys. vol. 80, pp. 2234-2252, 1996.

[10] Z. Stanojević, and H. Kosina, "Surface-roughness-scattering in non-planer channels – the role of band anisotropy," Proc. of SISPAD, pp. 352-355, 2013.